Robust Symbol and Frequency Synchronization Method for Burst OFDM Systems in UAV Communication

Lintao Li [1,*], Yue Han [2,3], Zongru Li [4], Hua Li [1], Jiayi Lv [4] and Yimin Li [4]

1 School of Computer and Communication Engineering, University of Science and Technology Beijing, Beijing 100083, China; lihua2023@ustb.edu.cn
2 School of Cyberspace Science and Technology, Beijing Institute of Technology, Beijing 100081, China; hanyue199910@163.com
3 Beijing Institute of Space Launch Technology, Beijing 100076, China
4 School of Information and Electronics, Beijing Institute of Technology, Beijing 100081, China; 3220220686@bit.edu.cn (Z.L.); 3120225408@bit.edu.cn (J.L.); 3220220687@bit.edu.cn (Y.L.)
* Correspondence: lilintao@ustb.edu.cn

Abstract: This paper introduces a robust synchronization method for orthogonal frequency division multiplexing (OFDM) in multi-unmanned aerial vehicle (UAV) communication systems, focusing on minimizing overhead while achieving reliable synchronization. The proposed synchronization scheme enhances both frame efficiency and implementation simplicity. Initially, a high-efficiency frame structure is designed without a guard time interval, utilizing a preamble sequence to simultaneously achieve both symbol synchronization and automatic gain control (AGC) before demodulation. Subsequently, a novel 2-bit non-uniform quantization method for the Zadoff–Chu sequences is developed, enabling the correlation operations in the traditional symbol synchronization algorithm to be implemented via bitwise exclusive OR (XOR) and addition operations. The complexity of hardware implementation and the energy consumption for symbol synchronization can be reduced significantly. Furthermore, the impact of AGC on frequency synchronization performance is examined, and an improved frequency synchronization method based on AGC gain compensation is proposed. Finally, the performance of the proposed method is rigorously analyzed and compared with that of the traditional method through computer simulations, demonstrating the effectiveness and superiority of the proposed approach.

Keywords: AGC compensation; synchronization; burst OFDM

1. Introduction

Unmanned aerial vehicles (UAVs), or drones, are highly maneuverable, low-cost, and rapidly deployable devices that have been widely used in various fields, including environmental monitoring [1], real-time monitoring of road traffic, search and rescue operations [2], mobile network deployment [3], and precision agriculture monitoring [4] in recent years. With the increasing complexity of mission execution, modes based on multi-drone collaborative control have been maturing [5]. Orthogonal frequency division multiplexing (OFDM) is a digital multi-carrier modulation method that divides the available spectrum into multiple orthogonal subcarriers. This approach can improve the frequency efficiency and provide strong resistance to multipath interference. With these characteristics, OFDM has become a prevalent choice in drone communications, demonstrating efficient and reliable data transmission [6,7]. To better meet the needs of different multi-UAV application scenarios, some integrated communication and sensing methods based on OFDM are presented in [8,9]. However, there is limited research on synchronization issues for OFDM in UAV communication networks.

Compared to traditional single-carrier systems, OFDM systems have stricter requirements for synchronization [10,11]. Symbol timing offset and frequency offset may introduce

significant inter-symbol and inter-carrier interference, adversely affecting bit error rate (BER) performance at the receiver. Therefore, accurate symbol and frequency synchronizations are essential for achieving reliable OFDM demodulation and optimal communication quality. When the OFDM is combined with frequency hopping technology [12,13] or used for time-division multiple access (TDMA) networking [14], a single communication process is short and bursty. In such scenarios, achieving low-complexity, fast, and reliable OFDM synchronization can be particularly challenging.

OFDM systems are significantly affected by multi-path propagation and the Doppler effect in UAV communication channels [15]. The received signal can vary over a large dynamic range becaused of path loss and small-scale fading. Consequently, an automatic gain control (AGC) circuit is generally required to adjust the received signal power before coherent demodulation. In the traditional burst OFDM frame design, an AGC guard interval is often introduced for power estimation and the adjustment of variable gain amplifier (VGA). Generally, the duration of the AGC guard interval should be longer than the setting time of the AGC, allowing the gain adjustment to be completed before the fast Fourier transform (FFT) demodulation. Otherwise, the subcarrier orthogonality would be compromised, leading to a degraded system performance [16,17]. Undoubtedly, the introduction of the AGC guard interval increases the overall time overhead, thus reducing the effective data transmission time within each frame. This inefficiency becomes more pronounced in bursty communication scenarios typical of UAV operations, where maintaining high data throughput is crucial. Therefore, optimizing the frame structure to minimize time overhead while ensuring reliable AGC adjustment is essential for improving the overall efficiency and performance of UAV communication systems [18].

Synchronization methods based on the Zadoff–Chu (ZC) sequences are widely used in real-world systems because of their ideal correlation properties [19]. Symbol timing synchronization is achieved through correlation operation and correlation peak searches between the received signal and a locally generated ZC sequence [20]. Additionally, frequency synchronization is accomplished by deriving the phase difference between adjacent training symbols [21]. Both synchronization algorithms require a number of complex multiplication operations that are linearly proportional to the length of the ZC sequence. Considering the energy limitations and processing ability constraints of UAVs, reducing the computational complexity of theses synchronization algorithms is crucial. Park reduced the computational complexity to a certain extent by designing a training sequence with symmetric characteristics and reducing the number of multiplication operations [22]. To achieve fast synchronization, preamble-based algorithms based on autocorrelation, cross-correlation, and their combination are proposed [23–25]. In [26], the local autocorrelation sequence was mapped into an elaborately simplified version, effectively halving the computational complexity. In [27], the hardware complexity was reduced by replacing the multipliers in a symmetric correlator with adders that compute the difference in magnitude between pairs of received samples. In [28], the elements of the training sequence were quantized to the nearest integer power of two, allowing the multiplication operation to be converted into a shift operation. In [29,30], the authors proposed a synchronization method based on 1-bit quantization. This method converts the multiplication operations in the correlation process into 1-bit addition operations, significantly reducing implementation complexity. However, this approach disregards the amplitude information of the training sequence, leading to a certain loss in synchronization performance. Most existing studies on OFDM synchronization assume that AGC adjustment is completed before the preamble of the transmission frame. While this assumption works well in continuous communication modes, in burst communication modes, a longer AGC settling time can lead to significant reductions in frame efficiency.

This work aims to address the aforementioned issues by developing a low-overhead frame structure, leveraging AGC control aided by symbol timing synchronization, and introducing robust synchronization methods for OFDM. These advancements collectively contribute to enhancing the frame efficiency and reliability of OFDM synchronization in

UAV communication channels. The main contributions of this paper are summarized as follows. (1) A more realistic frame structure with high transmission efficiency is designed. A novel AGC control circuit is developed based on the proposed model. (2) By introducing a 2-bit non-uniform quantization approach, the preamble for symbol timing synchronization can be quantized into a format represented by one sign bit and one amplitude bit. This allows synchronization correlation operations to be implemented with bitwise XOR and addition operations, resulting in low complexity. (3) To mitigate the impact of AGC-induced amplitude distortion on frequency synchronization performance, a novel frequency synchronization method based on AGC gain compensation is developed.

The rest of the paper is organized as follows. In Section 2, the system model and OFDM synchronization algorithms are introduced. In Section 3, a low-overhead frame for a burst OFDM system is designed. Based on the new frame, robust symbol and frequency synchronization algorithms are presented. In Section 4, the performances of the synchronization methods are analyzed. Finally, conclusions are drawn in Section 5.

2. System Model

2.1. Conventional Burst OFDM Frame Structure

The typical time slot arrangement for UAV networks based on time division duplexing–time division multiple access (TDD-TDMA) is illustrated in Figure 1. In this arrangement, each UAV (or user) is allocated a specific time slot for transmission, while the remaining UAVs are in the receiving mode during this period.
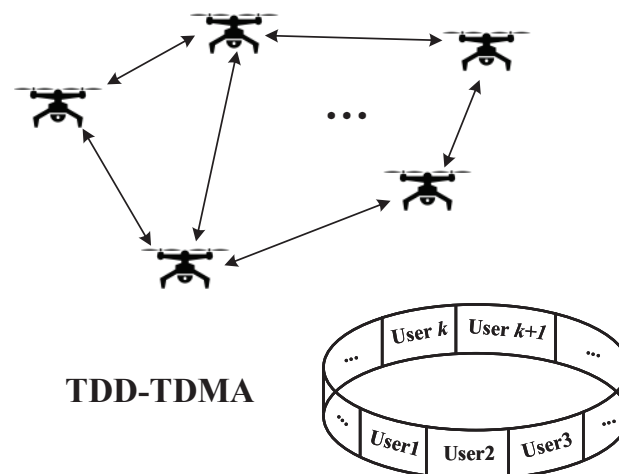

Figure 1. Time slot arrangement for an UAV network based on TDD-TDMA.

The conventional frame structure of a burst OFDM communication system is illustrated in Figure 2. The guard interval is used for path delay protection, and the AGC guard interval is used for received signal detection and AGC adjustment; the preamble is used for both symbol and frequency synchronization. The OFDM payload is the data area of the frame, which contains the valid data that are being sent. Therefore, the sum of T_G, T_{AGC}, and T_P is considered the time overhead for a single transmission. These parameters are determined by the communication distance, AGC convergence time, and synchronization performance requirements, respectively. When the time overhead $T_G + T_{AGC} + T_P$ is fixed, the proportion of overhead is larger when the total frame becomes shorter, which may severely reduce the data transmission efficiency. To address this issue, we need to design an efficient frame structure that can minimize the overhead proportion for a short-frame burst OFDM communication system.
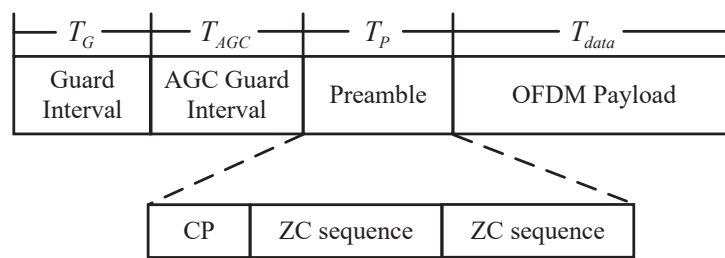
Figure 2. Traditional frame structure design.

2.2. Symbol and Frequency Synchronization Algorithms

The modulation and demodulation of the OFDM are implemented using inverse fast Fourier transform (IFFT) and fast Fourier transform (FFT). A symbol time synchronization should be performed to determine the start point of each OFDM symbol to take the FFT at the receiver end. Since the OFDM signal is sensitive to carrier frequency offset caused by the Doppler shift or local oscillator (LO) instabilities between the transmitter and the receiver, an accurate frequency synchronization estimation and compensation must be performed before demodulation. In a burst OFDM system, preamble-based symbol and frequency synchronization methods are commonly employed. Figure 2 illustrates an example of a preamble with a repetitive structure, where CP denotes the cyclic prefix. The fundamental concept is to leverage the good correlation characteristics of a training sequence. By correlating the received signal with the known training sequence at the receiver, a sharp correlation peak can be achieved. The Zadoff–Chu sequence can be defined as follows [19]:

$$
p_k(L, u, q) = \begin{cases} \exp\left(-j\frac{2\pi u}{L}\left(\frac{k^2}{2} + qk\right)\right), & \text{when } L \text{ is odd} \\ \exp\left(-j\frac{2\pi u}{L}\left(\frac{k(k+1)}{2} + qk\right)\right), & \text{when } L \text{ is even} \end{cases}, \tag{1}
$$

where j is the imaginary unit $j = \sqrt{-1}$, k is an integer time instant ranging from 0 to $L - 1$, L is the length of the ZC sequence, u is a root index that is prime to L, q is an arbitrary integer, and $q = 0$ in this work. The auto-correlation of ZC sequence with $L = 128$ and $u = 127$ is shown in Figure 3.
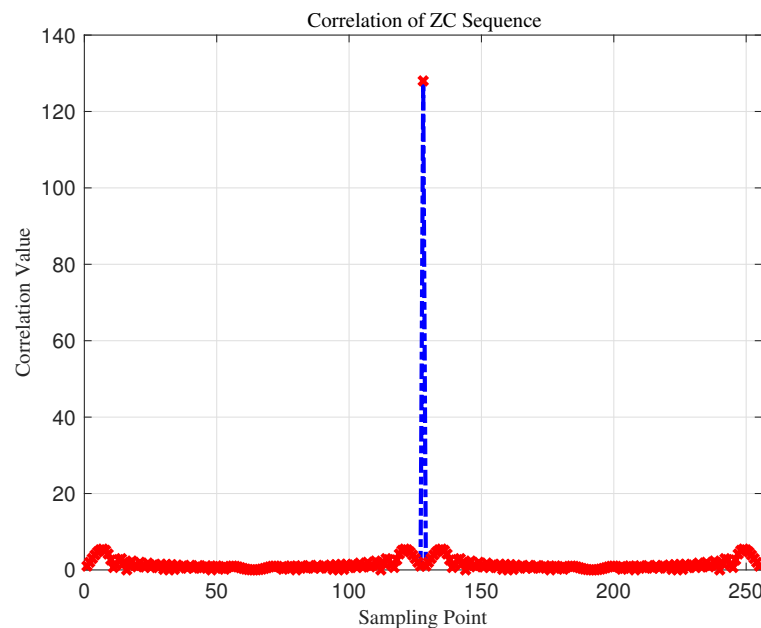

Figure 3. Autocorrelation of ZC sequence with length $L = 128$ in the (red) time and (blue) frequency domains.

Let $r(n)$ be the received signal at time n, and $s(k)$ be the known training sequence of length L. The complex correlation $V(n)$ can be expressed as [27]:

$$V(n) = \sum_{k=0}^{L-1} |r(n+k)s^*(k)|^2,$$ (2)

where $s^*(k)$ is the complex conjugate of $s(k)$. The presence of a preamble can be detected by comparing the correlation value with a pre-established threshold V_{th}, and as a result, an accurate position of the synchronization training sequence can be determined. According to Equation (2), the calculation of $V(n)$ requires L complex multiplication operations and $L-1$ addition operations, leading to high implementation complexity.

Additionally, the carrier frequency offset can be estimated from the phase angle of the product of a repetitive ZC sequence. For a given carrier frequency offset f_ω, the received signal can be expressed as:

$$r(n) = x(n)e^{j2\pi f_\omega n T_s} + w(n),$$ (3)

where $x(n)$ represents the transmission signal, T_s is the sampling period, and $w(n)$ denotes the noise component. The time-delayed autocorrelation of the two training symbols can be expressed as:

$$
\begin{aligned}
R &= \sum_{n=0}^{L-1} r(n)r^*(n+L) \\
&= \sum_{n=0}^{L-1} \Big[|x(n)|^2 e^{-j2\pi f_\omega L T_s} + x(n)e^{j(2\pi f_\omega n T_s + \varphi_0)} w^*(n+L) \\
&\quad + x^*(n+L)e^{-j(2\pi f_\omega (n+L)T_s + \varphi_0)} w(n) + w(n)w^*(n+L) \Big]
\end{aligned}
$$ (4)

where φ_0 denotes the initial phase offset between the transmitter and receiver. In the AWGN channel, the noise component $w(n)$ is modeled as a zero-mean independent and identically distributed Gaussian random variable. Therefore, the expectation value of product elements $x(n)e^{j(2\pi f_\omega n T_s + \varphi_0)} w^*(n+L)$, $x^*(n+L)e^{-j(2\pi f_\omega (n+L)T_s + \varphi_0)} w(n)$, and $w(n)w^*(n+L)$ are all zero. As a result, Equation (4) can be approximated as [23]

$$\hat{R} = e^{-j(2\pi f_\omega L T_s)} \sum_{n=0}^{L-1} |x_n|^2.$$ (5)

Therefore, the carrier frequency offset can be estimated by

$$\hat{f}_w = -\frac{1}{2\pi L T_s} \angle \hat{R},$$ (6)

where $\angle \hat{R}$ is the angle to $\hat{R}$. This technique can estimate the carrier frequency offset within the range $[-\Delta f, \Delta f]$.

3. Improved Burst OFDM Synchronization Method

In the traditional burst communication system, the AGC guard interval may introduce significant time overhead in a short-frame structure, resulting in low frame efficiency. If the AGC guard interval is eliminated, gain adjustment might occur during the preamble or the useful portion of the OFDM symbol. This can lead to a loss of subcarrier orthogonality, resulting in inter-carrier interference and significant performance degradation of the OFDM system [16]. Meanwhile, both low power consumption and miniaturization are essential for drones, thus necessitating that the hardware design and software processing algorithms of airborne equipment be as simple as possible. To address this, we propose a robust synchronization method that achieves a high frame efficiency with low complexity. The proposed method is analyzed from the perspectives of frame structure design, symbol time synchronization, and carrier frequency synchronization.

3.1. High-Efficiency Frame Structure Design

Frame efficiency is a measure of how effectively the available time slots within a frame are used for transmitting actual data, as opposed to overhead information such as synchronization or control signals. The frame efficiency is typically defined as the percentage of time slots in the frame that contain useful data. In this work, a novel low-overhead frame structure for a burst OFDM communication system is designed, as illustrated in Figure 4. Here, the AGC guard interval is eliminated, unlike in the traditional frame structure.
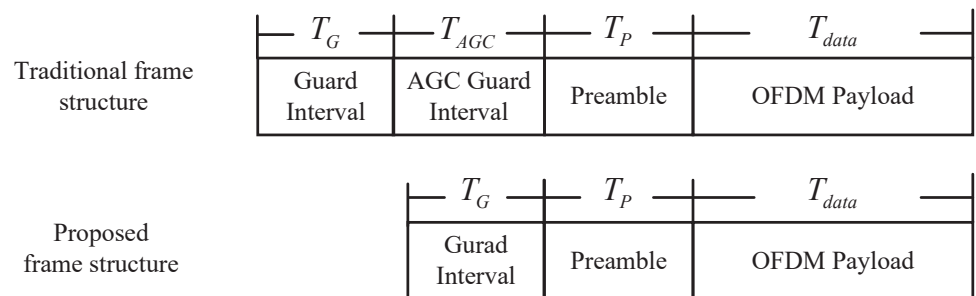
	T_G	T_{AGC}	T_P	T_{data}
Traditional frame structure	Guard Interval	AGC Guard Interval	Preamble	OFDM Payload

	T_G	T_P	T_{data}
Proposed frame structure	Gurad Interval	Preamble	OFDM Payload

Figure 4. The proposed frame structure and its comparison with the traditional frame structure.

Hence, the frame efficiency of the traditional frame structure can be expressed by

$$\eta = \frac{T_{data}}{T_G + T_{AGC} + T_P + T_{data}}, \tag{7}$$

and the frame efficiency of the proposed frame structure is

$$\eta' = \frac{T_{data}}{T_G + T_P + T_{data}}. \tag{8}$$

The proposed frame structure can improve the frame efficiency by

$$\Delta\eta = \frac{T_{data}T_{AGC}}{(T_G + T_P + T_{data})(T_G + T_{AGC} + T_P + T_{data})}, \tag{9}$$

when T_p and T_{AGC} in Equations (7) and (8) are fixed.

The power of the received preamble may vary over a large dynamic range since the AGC guard interval is eliminated. To regulate the power of the received signal to a desired level before receiving the OFDM payload symbols, we present an AGC strategy based on the symbol synchronization result. The block diagram of the proposed AGC control circuit is illustrated in Figure 5.

The VGA is used to amplify or attenuate the received signal. The average power calculator computes the mean power of the received signal, which is then compared with a preset reference power and fed into a VGA control module. The VGA control module calculates the VGA adjustment step based on the power difference between the received signal power and the reference power. The control switch governed by the result of the symbol timing synchronization determines whether to update the VGA. A successful symbol synchronization indicates that the preamble has been detected; if so, the control switch is turned off, and the VGA does not need to adjust the gain. Otherwise, the control switch is turned on, and the VGA works according to the VGA control word generated by the VGA control module. With this strategy, the receiver can stop the VGA adjustment after detecting the preamble, thereby reducing frame overhead and improving reception efficiency.
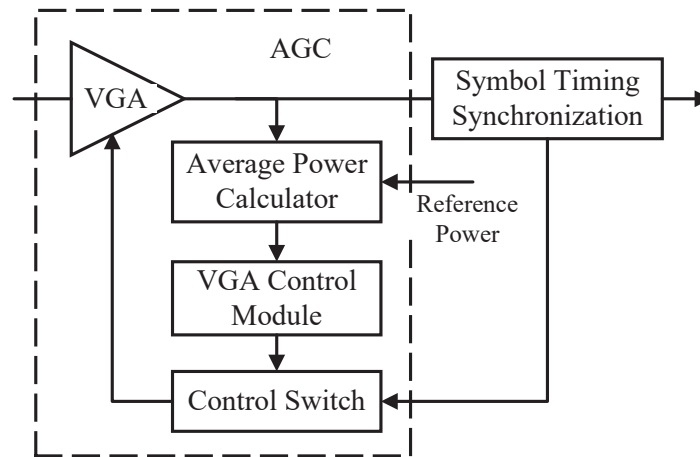
Figure 5. Block diagram of the proposed AGC control circuit.

3.2. Symbol Timing Synchronization Method Based on 2-Bit Non-Uniform Quantization

This study proposes an improved synchronization algorithm based on 2-bit non-quantization to achieve accurate symbol timing synchronization with low computational complexity. The computation complexity is significantly reduced by replacing the complex multiplications in correlation processing with XOR and addition operations. This approach preserves crucial signal information while minimizing any loss in synchronization accuracy by carefully designing the quantization levels. We need to clarify that the proposed non-uniform quantization method is only applied during the symbol synchronization process. In the subsequent signal processing steps, such as channel estimation, equalization, and channel decoding, the traditional uniform quantization method is employed.

3.2.1. The 2-Bit Non-Uniform Quantization Method

In this work, the received signal and the local training sequence are mapped to a 2-bit message comprising a sign bit and a magnitude bit. The quantization method can be expressed as $\hat{r}(n) = \{a_n, b_n\}$, where a_n and b_n are binary values representing the sign and magnitude bit of the quantization, respectively. The quantization rules can be expressed as

$$a_n = \begin{cases} 0, & \hat{r}(n) \geq 0 \\ 1, & \hat{r}(n) < 0 \end{cases}, \tag{10}$$

$$b_n = \begin{cases} 0, & |\hat{r}(n)| < T_{th} \\ 1, & |\hat{r}(n)| \geq T_{th} \end{cases}, \tag{11}$$

where T_{th} is the optimized threshold for quantization. $b_n = 1$ implies that the amplitude of $\hat{r}(n)$ is quantized to a higher value T_1, and $b_n = 0$ implies that the amplitude of $\hat{r}(n)$ is quantized to a lower value T_0. Here, T_0 and T_1 are optimized mapping values, which are analyzed in the following sections. Let $\hat{r}_n^I$ and $\hat{r}_n^Q$ denote the real and imaginary parts of $\hat{r}_n$, which will be quantized into $\left\{ a_{r_n}^I, b_{r_n}^I \right\}$ and $\left\{ a_{r_n}^Q, b_{r_n}^Q \right\}$, respectively. Similarly, the real part (s_n^I) and imaginary part (s_n^Q) of the local training sequence at the receiving end are quantized into $\left\{ a_{s_n}^I, b_{s_n}^I \right\}$ and $\left\{ a_{s_n}^Q, b_{s_n}^Q \right\}$, respectively.

3.2.2. Low-Complexity Timing Synchronization Method

Based on the quantization method presented in the previous section, the complex multiplication in Equation (2) can be expressed as follows:

$$
\begin{aligned}
c_{n,k} &= \hat{r}_{n+k}s_k^* \\
&= \left(\hat{r}_{n+k}^I + j\hat{r}_{n+k}^Q\right)\left(s_k^I - js_k^Q\right) \\
&= \hat{r}_{n+k}^I s_k^I + \hat{r}_{n+k}^Q s_k^Q + j\left(\hat{r}_{n+k}^Q s_k^I - \hat{r}_{n+k}^I s_k^Q\right)
\end{aligned}
\tag{12}
$$

Let $c_1 = \hat{r}_{n+k}^I s_k^I$, $c_2 = \hat{r}_{n+k}^Q s_k^Q$, $c_3 = \hat{r}_{n+k}^Q s_k^I$, and $c_4 = \hat{r}_{n+k}^I s_k^Q$. We can determine the signs of these variables as

$$
\begin{cases}
a_{c_1} = a_{\hat{r}_{n+k}^I} \oplus a_{s_k^I} \\
a_{c_2} = a_{\hat{r}_{n+k}^Q} \oplus a_{s_k^Q} \\
a_{c_3} = a_{\hat{r}_{n+k}^Q} \oplus a_{s_k^I} \\
a_{c_4} = a_{\hat{r}_{n+k}^I} \oplus a_{s_k^Q}
\end{cases},
\tag{13}
$$

where $\oplus$ represents a bitwise XOR operation. The magnitudes of these variables are expressed as

$$
\begin{cases}
b_{c_1} = b_{\hat{r}_{n+k}^I} + b_{s_k^I} \\
b_{c_2} = b_{\hat{r}_{n+k}^Q} + b_{s_k^Q} \\
b_{c_3} = b_{\hat{r}_{n+k}^Q} + b_{s_k^I} \\
b_{c_4} = b_{\hat{r}_{n+k}^I} + b_{s_k^Q}
\end{cases}.
\tag{14}
$$

The calculated result $b_{c_i}(i = 1, 2, 3, 4)$ is represented by two bits 00,01,10, and the corresponding real values are as shown in Table 1. Since $0 < T_0 < T_1$, we can conclude that $T_0^2 < T_0 T_1 < T_1^2$.

Table 1. A 2-bit magnitude representation and their real value.

$b_{c_i}(i = 1, 2, 3, 4)$	Magnitude
00	T_0^2
01	$T_0 T_1$
10	T_1^2

As a result, the variables $c_i(i = 1, 2, 3, 4)$ can be represented with 3 bits as $\{a_{c_i}, b_{c_i}\}$. However, the 3-bit result cannot be used directly when calculating $c_k^I = c_1 + c_2$ and $c_k^Q = c_3 - c_4$. They should be mapped to the true value before the addition operation. The specific calculation method can be expressed as

$$
c_{n,k} = f(c_1) + f(c_2) + j(f(c_3) - f(c_4)),
\tag{15}
$$

where the reconstruction function is defined by

$$
f(c_i) = \begin{cases}
(1 - 2a_{c_i})T_0^2, & b_{c_i} = \text{`00'} \\
(1 - 2a_{c_i})T_0 T_1, & b_{c_i} = \text{`01'} \\
(1 - 2a_{c_i})T_1^2, & b_{c_i} = \text{`10'}
\end{cases}.
\tag{16}
$$

Therefore, $c_{n,k}$ can be computed using XOR and addition operations instead of complex multiplication operations. By substituting it into Equation (2), we can obtain the instantaneous correlation value $V(n)$. A decision can be made to determine the starting position of the OFDM symbol by comparing V_n to the pre-established threshold V_{th}. It should be noted that the performance of the proposed symbol timing synchronization method based on 2-bit non-uniform quantization depends largely on the selection of the

threshold V_{th} and mapping values T_0 and T_1. In this study, an optimal search method for these parameters based on the information rate distortion function is presented.

3.2.3. Search Method Based on Distortion Function

According to the quantization method described in the previous section, the information rate distortion is chosen as the optimization objective. To find the optimal quantization parameters, a traversal method is used to search through all possible combinations of these parameters. The squared error distortion function of a sequence is used to represent the information distortion [31], and it is defined by

$$d(\mathbf{s}, \tilde{\mathbf{s}}) = \frac{1}{L} \sum_{k=0}^{L-1} d(s_k, \tilde{s}_k), \tag{17}$$

where s_k represents the original signal value and $\tilde{s}_k$ represents the quantized signal value. This distortion function allows us to quantify the information loss due to quantization and find the optimal set of quantization parameters that minimize this loss. Algorithm 1 outlines the steps to find the optimal non-uniform quantization parameters.

Algorithm 1 Optimal parameter search algorithm for 2-bit non-uniform quantization

---

1: **Input:** $\mathbf{s} = s_k (1 \le k \le L)$.
2: **Initialization:** *Set search step size* Δ, *and the initial threshold* $T_{th} = \Delta$.
3: **Step1:** Compute the maximum magnitude of the real and imaginary parts of the training sequence $\mathbf{s}$ using $T_{\max} = \max\left(\max(|s_k^I|) \max\left(|s_k^Q|\right)\right)$ for all $k (1 \le k \le L)$;
4: **Step2:** For all $\{T_0, T_1\}$ that $T_0 \in [0, T_{th})$ and $T_1 \in [T_{th}, T_{max}]$, quantize $\mathbf{s}$ using (10) and (11), and compute the corresponding distortion $d(\mathbf{s}, \tilde{\mathbf{s}})$;
5: **Step3:** Find the minimum distortion $d_{min,T_{th}}$ and the corresponding parameter combination as $\{T_0^*, T_1^*\} = \underset{T_0 \in [0,T_{th}), T_1 \in [T_{th}, T_{\max}]}{\arg\min} d(\tilde{\mathbf{s}}, T_0, T_1)$;
6: **Step4:** Repeat Steps 2 to 3 with updated threshold $V_{th} = V_{th} + \Delta$ until $V_{th} = T_{max}$;
7: **Step5:** Compute the minimum distortion value d_{min} among $\{d_{min,T_{th}}, T_{th} \in [0, T_{\max}]\}$, and return the corresponding optimal parameters $T_{th,opt}$, $T_{0,opt}$, and $T_{1,opt}$.

3.2.4. Computational Complexity Analysis

This section analyzes the computational complexity to evaluate the advantages of the proposed symbol timing synchronization method in hardware implementation. The main computational complexity of the symbol synchronization lies in the calculation of the correlation value between the received signal and the local training sequence. The traditional calculation of V_n requires $4L$ multiplication operations and $4L - 1$ addition operations for each sampling point. The computational complexity reduces to $4L$ XOR operations and $4L - 1$ addition operations for the synchronization method based on 1-bit quantization. However, this method ignores the magnitude information, resulting in significant synchronization performance loss. In contrast, when the 2-bit quantization method is used, the simplified calculation method given by Equations (13) and (14) can be used, wherein the calculation of $V(n)$ requires $4L$ XOR operations and $8L - 1$ addition operations. In practical systems, a larger bit width is necessary to achieve good synchronization performance. Meanwhile, the hardware implementation complexity increases linearly with the bit width. The computational complexity comparison of different correlation operations is shown in Table 2. The proposed symbol synchronization based on the 2-bit non-uniform quantization method performs well in computational complexity.

Table 2. Computational complexity comparison of different calculation methods of the correlation value.

	Traditional Method	1-bit Quantization	2-bit Uniform Quantization	Proposed Method
Multiplication	$4L$	0	0	0
Addition	$4L - 1$	$4L - 1$	$8L - 1$	$8L - 1$
XOR	0	$4L$	$4L$	$4L$

3.3. Frequency Synchronization Algorithm Based on AGC Gain Compensation

3.3.1. AGC Impact Analysis for Low-Overhead Frame Structure

In conventional burst OFDM systems, the AGC gain adjustment is completed within the AGC guard interval. Otherwise, the input signal for frequency synchronization may suffer amplitude distortion, potentially leading to significant performance loss. When the frame structure design illustrated in Figure 4 is used, the AGC gain adjustment is carried out within the preamble. The relationship between the received signal before and after AGC adjustment can be expressed as

$$\gamma(n) = g(n)r(n), \tag{18}$$

where $g(n)$ denotes the AGC gain. In practical systems, the AGC adjustment step is controlled by the power of received signal samples, and we convert the gain $g(n)$ into dB by

$$G(n)_{dB} = 20 \log_{10} g(n). \tag{19}$$

The AGC gain is changed from an initial value $G(i)_{dB}$ to a steady-state value, and the gain $G(n)$ is updated with step λ_k for time interval τ. The AGC gain $G(n)_{dB}$ at each moment n can be expressed as

$$G(n) = G(i)u(n) + \sum_{k=0}^{K-1} \lambda_k u(n - k\tau), \tag{20}$$

where $G(i)_{dB}$ denotes the initial gain of the AGC and $u(n)$ is the unit step function. The overall convergence time of the AGC is determined by the gain-adjusted time interval τ and gain adjustment step λ_k.

Figure 6 shows an example of the received preamble with AGC adjustment, where I and Q denote the in-phase and quadrature components of ZC sequence, respectively. The preamble consists of two ZC sequences, each with a length of 128, and a CP with a length of 64. The time domain waveform of the received signal after the AGC adjustment is illustrated in Figure 7. When the preamble is not present, the received signal only contains noise at a low power level. The AGC gain is initially set to the maximum value and gradually decreases so that the received signal power reaches the reference power. Therefore, an overload occurs within the CP at the very beginning of the preamble.

3.3.2. Frequency Synchronization Scheme Based on AGC Compensation

To mitigate the frequency synchronization performance loss due to gain adjustment in burst OFDM systems, we introduce a robust frequency synchronization based on AGC compensation. The diagram of the proposed synchronization method is illustrated in Figure 8.
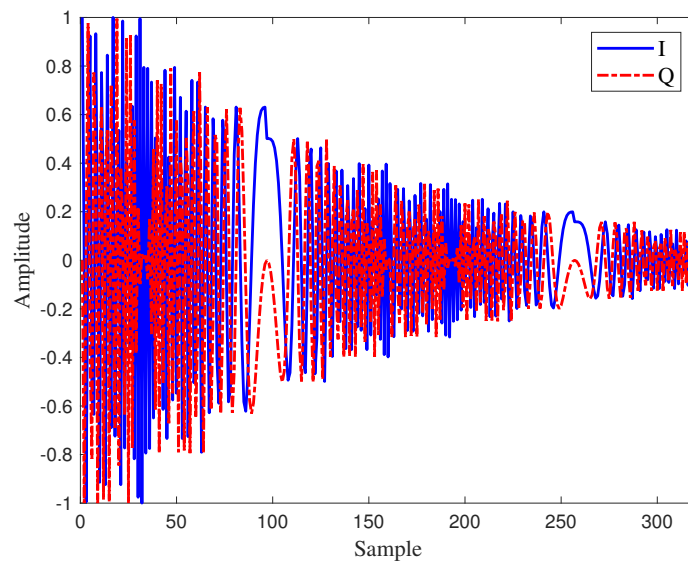
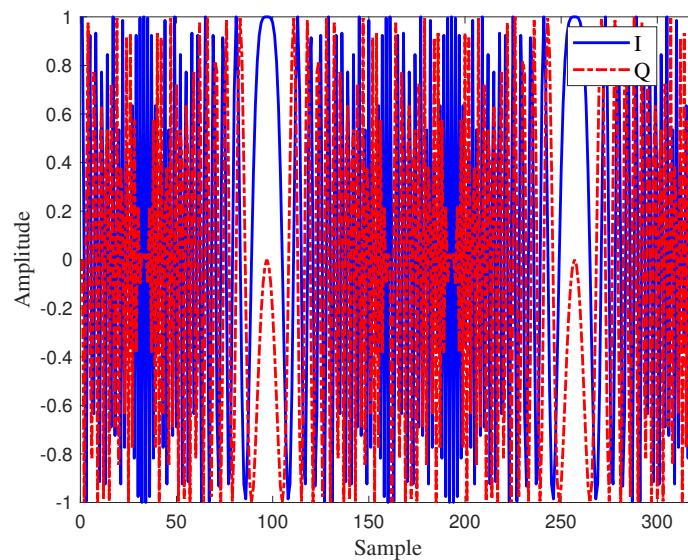**Figure 6.** Time domain waveform of preamble after AGC adjustment.

Figure 7. Time domain waveform of preamble after AGC compensation.

An amplitude compensation module is introduced between the symbol timing synchronization and frequency offset estimation modules. The AGC gain value $G(n)$ is not only sent to the VGA but also to the amplitude compensation module. The symbol timing synchronization is complete when the cross-correlation value $V(n)$ exceeds the synchronization threshold V_{th}. Therefore, the accurate position of the preamble and the gain $G(n)_{dB}$ for each sample is known before frequency synchronization. We can multiply the output signal of the AGC module by a coefficient so that it maintains a constant power over the entire duration.

The amplitude compensation method can be expressed as

$$
\begin{aligned}
\hat{\gamma}(n) &= 10^{\frac{G_{ref}-G(n)}{20}}\gamma(n) \\
&= \frac{g_{ref}}{g(n)}\gamma(n)
\end{aligned}
\tag{21}
$$

where G_{ref} denotes the AGC gain that adjusts the received signal power to approach the given reference power. The time domain waveform of the compensated signal $\hat{\gamma}(n)$ is

illustrated in Figure 7, showing that the distorted preamble is transformed into a distortion-free preamble when the channel noise is absent.
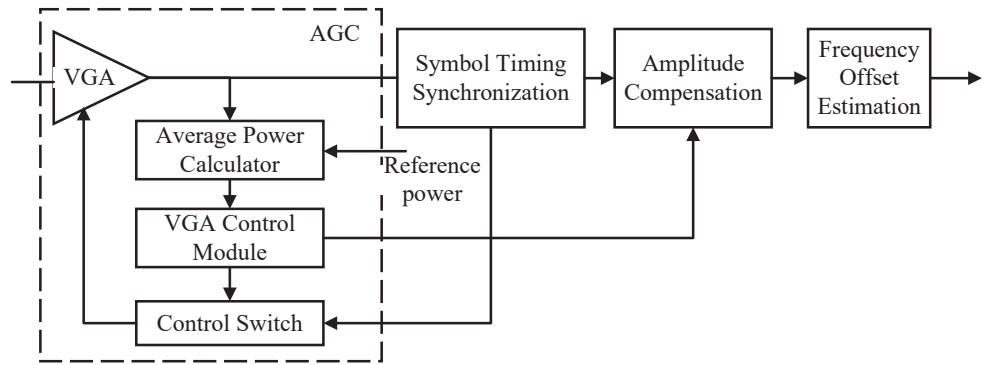

Figure 8. Block diagram of frequency synchronization scheme based on AGC compensation.

With the compensated training sequences within the preamble, we can rewrite Equation (4) as

$$
\begin{aligned}
\hat{R} &= \sum_{n=0}^{L-1} \hat{\gamma}(\hat{n}+n)\hat{\gamma}^*(\hat{n}+n+L) \\
&= e^{-(j2\pi f_w L T_s)} \sum_{n=0}^{L-1} g_{ref}^2 |x(n)|^2
\end{aligned}
, \tag{22}
$$

where $\hat{n}$ denotes the accurate start position of the synchronized preamble. Using Equation (6), we can determine the estimated frequency offset $\hat{f}_w$.

4. Performance Analysis

4.1. Symbol Timing Synchronization Performance

In this section, the symbol timing synchronization performance is evaluated in terms of detection probability. In the simulations, a ZC sequence with length $L = 128$ and root index $u = 127$ is employed. The sub-carrier spacing is 15 kHz; hence, the bandwidth of the preamble is 1.92 MHz. For the additive white Gaussian noise (AWGN) channel, the received signal can be given in the following composite model:

$$
\begin{cases}
\mathcal{H}_0 : r(n) = w(n) \\
\mathcal{H}_1 : r(n) = s(n) + w(n)
\end{cases}
, \tag{23}
$$

where $\mathcal{H}_0$ represents the null hypothesis in which the preamble is not present and $\mathcal{H}_1$ represents the alternative hypothesis in which the preamble is present. In this work, a correlator is considered at the receiver end, and thus, the decision rule can be written as

$$
V(n) \underset{\mathcal{D}_1}{\overset{\mathcal{D}_0}{\lessgtr}} V_{th}, \tag{24}
$$

where $\mathcal{D}_0$ and $\mathcal{D}_1$ are decisions that a preamble exists or not, respectively. In the context of symbol timing synchronization, the detection performance is evaluated based on detection probability $P_d \overset{\Delta}{=} \Pr(\mathcal{D}_1|\mathcal{H}_1)$ and false alarm probability $P_{fa} \overset{\Delta}{=} \Pr(\mathcal{D}_1|\mathcal{H}_0)$.

When $\mathcal{H}_0$ is true, the received signal is a Gaussian sequence with a zero mean. Following Equations (2) and (23), the probability density function (PDF) of the correlation can be expressed as [32]

$$
f(z|H_0) = \frac{1}{2\sigma^2} \exp\left(-\frac{z}{2\sigma^2}\right), z \geq 0, \tag{25}
$$

where $2\sigma^2 = L \cdot N_0$, L is the training sequence's length, and N_0 is the noise power spectral density.

Consequently, the false alarm probability is expressed by

$$P_{fa} = \int_{V_{th}}^{+\infty} f(z|\mathrm{H}_0)dz \approx \exp\left(-\frac{V_{th}}{2\sigma^2}\right). \tag{26}$$

According to Equation (26), V_{th} can be expressed as an inverse function of P_{fa}:

$$V_{th} = -2\sigma^2 \ln(P_{fa}). \tag{27}$$

Moreover, the correlation value $V(n)$ is subject to a non-central χ^2 distribution when $\mathcal{H}_1$ is true, and the PDF of $V(n)$ can be expressed as

$$f(z|\mathrm{H}_1) = \frac{1}{2\sigma^2} \exp\left(\frac{z+L^2}{2\sigma^2}\right) I_0\left(\frac{L\sqrt{z}}{\sigma^2}\right), z \geq 0. \tag{28}$$

As a result, the detection probability P_d can be expressed as

$$P_d = \int_{V_{th}}^{+\infty} f(z|\mathrm{H}_1)dz = \mathrm{Q}\left(\sqrt{2L \times SNR}, \sqrt{-2\ln(P_{fa})}\right), \tag{29}$$

where SNR is the signal-to-noise ratio of the received signal and $\mathrm{Q}(a,b)$ is the Marcum Q-function defined by

$$\mathrm{Q}(a,b) = \int_{b}^{+\infty} x \exp\left(-\frac{x^2+a^2}{2}\right) I_0(ax)dx. \tag{30}$$

4.2. Frequency Synchronization Performance Analysis

To verify the effectiveness and performance of the AGC compensation method, we compare the error vector measure (EVM) of the preamble with and without AGC compensation. The EVM is used to quantify the signal distortion and is defined as

$$EVM = \sqrt{\frac{\sum\limits_{k=1}^{L}\left[\left(I_k - \tilde{I}_k\right)^2 + \left(Q_k - \tilde{Q}_k\right)^2\right]}{\sum\limits_{k=1}^{L}\left(I_k^2 + Q_k^2\right)}}, \tag{31}$$

where I_k and Q_k represent the real and imaginary parts of the original training sequence, respectively, and $\tilde{I}_k$ and $\tilde{Q}_k$ represent the real and imaginary parts of the quantized training sequence, respectively.

Furthermore, the frequency synchronization performance is evaluated using the normalized mean square error (NMSE) of frequency estimation, which is defined by

$$NMSE \triangleq \frac{\sum\limits_{m=1}^{M}\left[\left(\hat{f}_{w,m} - f_w\right)\right]^2}{Mf_w^2}, \tag{32}$$

where M is the number of simulation runs, and $\hat{f}_{w,m}$ is the frequency offset estimate obtained from the m-th simulation run.

5. Simulation Results

5.1. Distortion Measures for Non-Uniform Quantization

In this subsection, we analyze the relationship between the threshold V_{th} and the corresponding minimum distortion value $d(\mathbf{s}, \tilde{\mathbf{s}})$. Figures 9 and 10 illustrate the minimum distortion between the original training sequence and the quantized version when different quantization methods are employed. In the simulations, we use the ZC sequences with

length $L = 128$ and root indexes $u = 127$, $u = 85$. The search step is set to $\Delta = 0.02$ to obtain the optimal mapping values T_0 and T_1 using Algorithm 1.
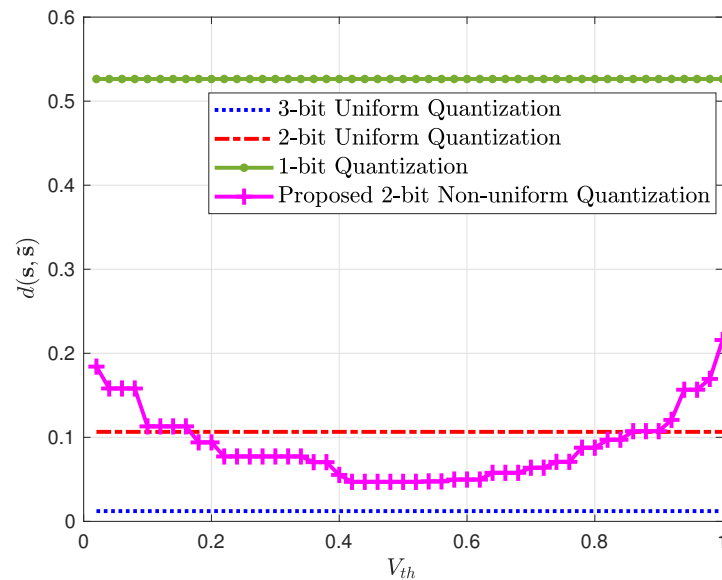

Figure 9. Distortion function of quantized ZC sequence with different quantization methods ($L = 128$, $u = 127$).
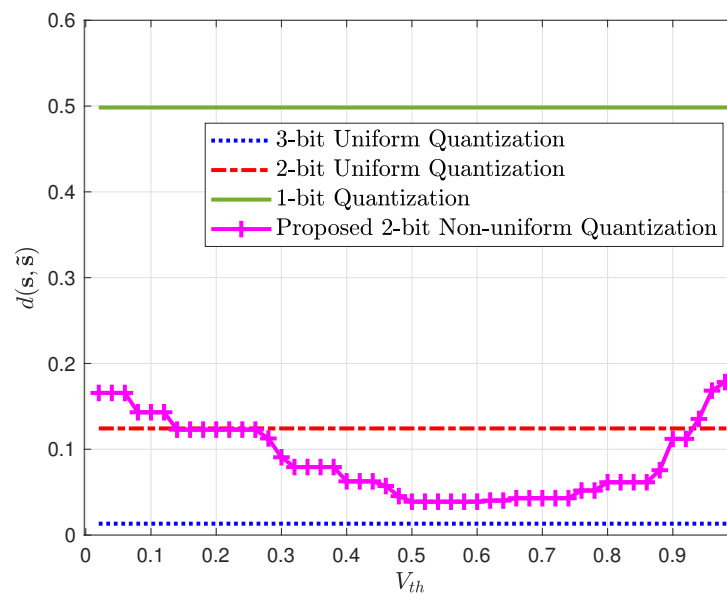

Figure 10. Distortion function of quantized ZC sequence with different quantization methods ($L = 128$, $u = 85$).

Based on Figures 9 and 10, we can conclude that a larger quantization bit width leads to a smaller distortion $d(\mathbf{s}, \tilde{\mathbf{s}})$. Unlike uniform quantization methods, the performance of the proposed 2-bit non-uniform quantization method varies with different V_{th}. For the ZC sequence with a root index $u = 127$, as shown in Figure 9, the minimum distortion $d(\mathbf{s}, \tilde{\mathbf{s}})$ is 0.047 when $T_{th} = 0.42$, $T_0 = 0.2$, and $T_1 = 0.84$. For the ZC sequence with a root index $u = 85$, as shown in Figure 10, the minimum distortion $d(\mathbf{s}, \tilde{\mathbf{s}})$ is 0.039 when $T_{th} = 0.5$, $T_0 = 0.28$, and $T_1 = 0.88$. This reveals that the optimal parameters for ZC sequences with different root indexes u are also different. The simulation results also indicate that the proposed non-uniform quantization scheme performs better than the

uniform quantization method with the same bit width and is nearly as effective as the 3-bit uniform quantization method.

It is well known that symbol synchronization based on preamble sequences is achieved by finding correlation peaks. Therefore, the peak-to-average ratio of the correlation results can be used as one of the metrics to evaluate the sequence synchronization performance. In our previous work [32], the feasibility of reducing complexity through non-uniform quantization of the preamble sequence has already been verified. In that work, the peak-to-average ratio (PAR) is used as the cost function for searching the optimal non-uniform quantization parameters. Therefore, we also evaluate the correlation characteristic of the quantized ZC sequence by analyzing the PAR of the autocorrelation function in this work. Simulation results are shown in Figures 11 and 12 with ZC sequences with length $L = 128$ and root indexes $u = 127$ and $u = 85$. The simulations show that the minimum distortion $d(\mathbf{s}, \tilde{\mathbf{s}})$ and the maximum PAR are obtained with the same parameter V_{th}.
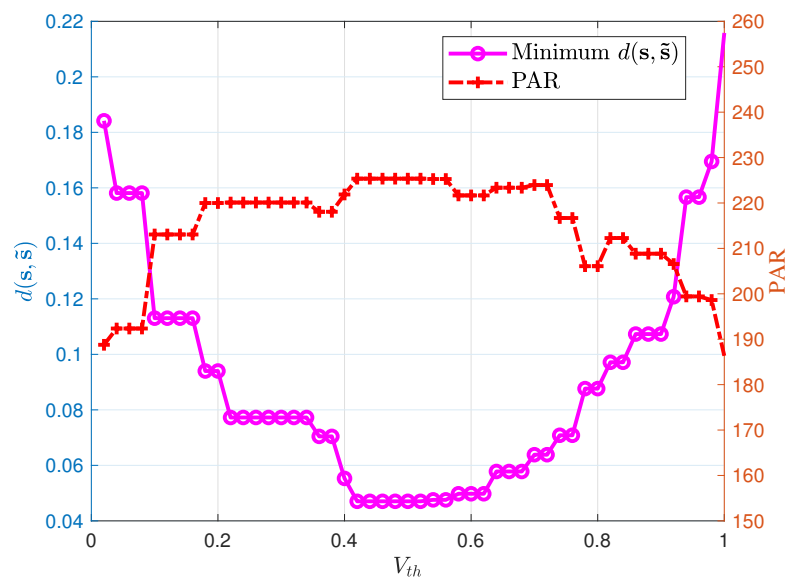

Figure 11. Distortion and PAR of the ZC sequence with 2-bit non-uniform quantization ($L = 128$, $u = 127$).
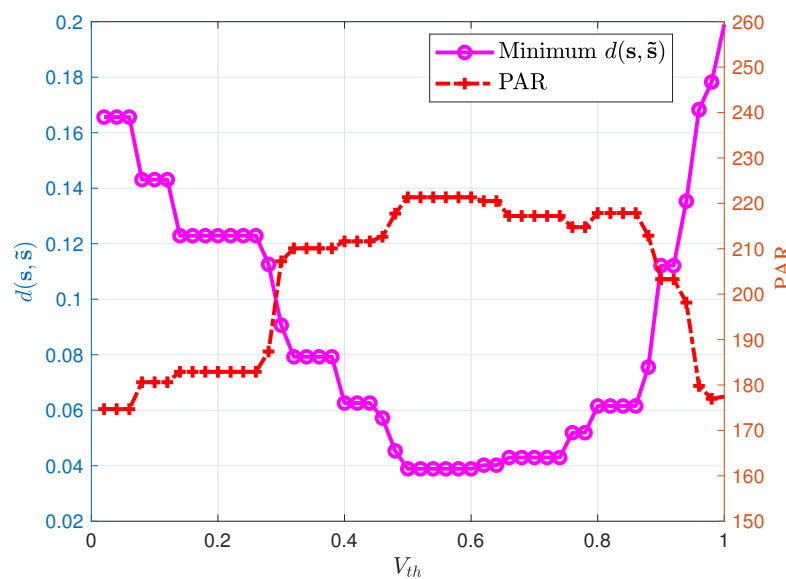

Figure 12. Distortion and PAR of the ZC sequence with 2-bit non-uniform quantization ($L = 128$, $u = 85$).

5.2. Symbol Synchronization Performance

In this work, we assume that constant false alarm ratio detection is employed and set $P_{fa} = 10^{-4}$. The threshold V_{th} is dynamically calculated using Equation (27). The symbol timing synchronization performance with different quantization methods is illustrated in Figure 13. The numerical result provides a theoretical analysis for the detection probability using Equation (29), which matches well with the floating-point simulation result. For the uniform quantization methods, the detection performance increases with the quantization bit width. The proposed 2-bit non-uniform quantization method performs nearly the same as the theoretical approach in the high-SNR region ($SNR \geq -6$ dB). For a given detection probability, the proposed 2-bit non-uniform quantization method is approximately 2 dB better than the 2-bit uniform quantization method. As a result, the effectiveness and superiority of the proposed scheme are demonstrated.
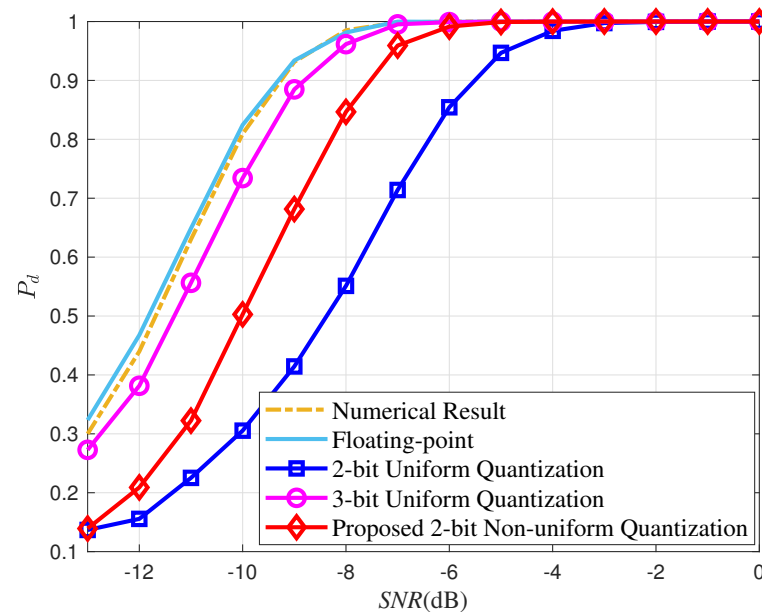

Figure 13. Comparison of symbol timing synchronization performance over AWGN channel with different quantization methods.

5.3. Frequency Synchronization Performance

In the simulations, a ZC sequence with length $L = 128$ and a root index $u = 127$ is employed. The symbol timing synchronization is assumed to be perfect. The AGC gain is adjusted with a gain step $\lambda = 2$ dB for every $\tau = 16$ samples. The comparison of EVM for the preamble with frequency offsets 300 Hz and 450 Hz is illustrated in Figure 14. The simulation results allow us to assess the effectiveness of the proposed AGC compensation method in reducing distortion and improving signal quality.

The comparison of NMSE for the frequency estimation with and without AGC compensation is illustrated in Figure 15. In the simulations, the frequency offset is set to 300 Hz and 450 Hz, and the AWGN channel is considered. The simulation results show that the proposed frequency synchronization scheme improves the performance by approximately 2 dB.
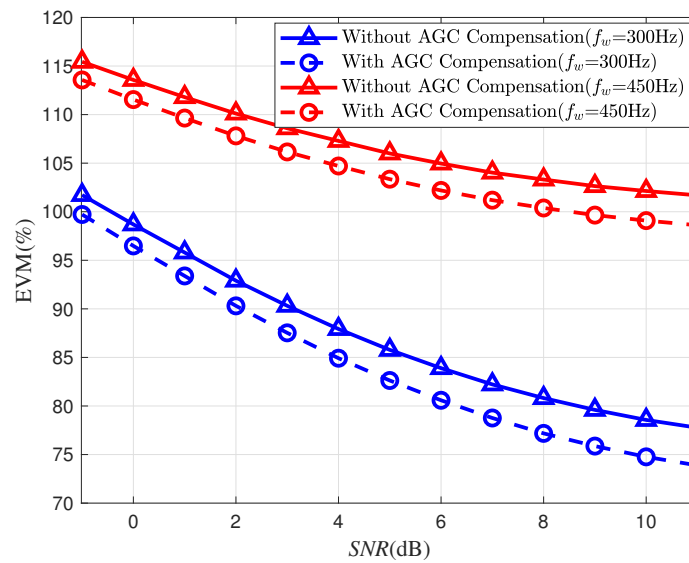
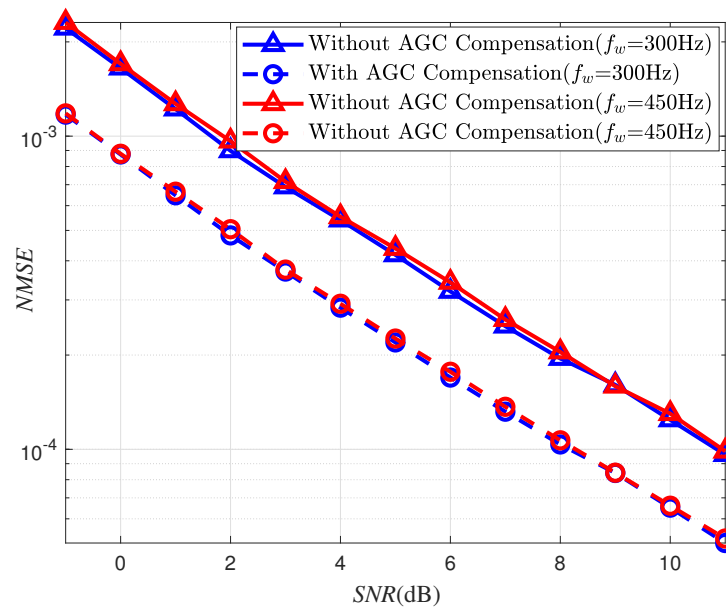**Figure 14.** EVM of the preamble with and without AGC compensation.

Figure 15. Performance comparison of frequency offset estimation with and without AGC compensation.

6. Conclusions

This paper develops a low-overhead frame structure design and robust symbol timing and frequency synchronization methods for OFDM systems used in UAV TDD-TDMA communication networks. First, we achieve a high-efficiency transmission frame by eliminating the AGC guard interval. We also introduce a novel AGC circuit that is controlled by the results of symbol timing synchronization. Second, we propose a symbol timing synchronization algorithm based on 2-bit non-uniform quantization, where the training sequence is mapped into a 2-bit message, represented by a sign bit and a magnitude bit. We also introduce an optimal quantization parameter search algorithm based on minimum distortion. This approach allows the correlation operation in symbol synchronization to be implemented using bitwise XOR and addition operations, significantly reducing the hardware implementation complexity. Third, we present a robust frequency offset estimation algorithm based on AGC compensation to mitigate the destructive effects of AGC

adjustment on frequency synchronization. The simulation results demonstrate that the proposed 2-bit symbol timing synchronization achieves performance nearly equivalent to traditional 3-bit uniform quantization. Additionally, the frequency estimation performance is improved by approximately 2 dB using AGC compensation. Following the main results presented here, a near future work is to extend the current system to more realistic scenarios by considering the inclusion of multipath fading or interference.

Author Contributions: Conceptualization, L.L.; methodology, Y.H. and Z.L.; validation, Y.H., Z.L. and J.L.; formal analysis, H.L.; writing—original draft preparation, L.L.; writing—review and editing, Y.L. and J.L.; supervision, L.L.; funding acquisition, H.L. All authors have read and agreed to the published version of the manuscript.

Data Availability Statement: The raw data supporting the conclusions of this article will be made available by the authors on request.

Conflicts of Interest: The authors declare no conflicts of interest.

References

1. Bushnaq, O.M.; Chaaban, A.; Al-Naffouri, T.Y. The role of UAV-IoT networks in future wildfire detection. *IEEE Internet Things J.* **2021**, *8*, 16984–16999. [CrossRef]
2. Ghamari, M.; Rangel, P.; Mehrubeoglu, M.; Tewolde, G.S.; Sherratt, R.S. Unmanned Aerial Vehicle Communications for Civil Applications: A Review. *IEEE Access* **2022**, *10*, 102492–102531. [CrossRef]
3. Zeng, Y.; Zhang, R.; Lim, T.J. Wireless communications with unmanned aerial vehicles: Opportunities and challenges. *IEEE Commun. Mag.* **2016**, *54*, 36–42. [CrossRef]
4. Murugan, D.; Garg, A.; Singh, D. Development of an adaptive approach for precision agriculture monitoring with drone and satellite data. *IEEE J. Sel. Topics Appl. Earth Observ. Remote Sens.* **2017**, *10*, 5322–5328. [CrossRef]
5. Alotaibi, E.T.; Alqefari, S.S.; Koubaa, A. LSAR: Multi-UAV collaboration for search and rescue missions. *IEEE Access* **2019**, *7*, 55817–55832. [CrossRef]
6. Lu, W.; Si, P.; Gao, Y.; Han, H.; Liu, Z.; Wu, Y.; Gong, Y. Trajectory and Resource Optimization in OFDM-Based UAV-Powered IoT Network. *IEEE Trans. Green Commun. Networking* **2021**, *5*, 1259–1270. [CrossRef]
7. Gupta, L.; Jain, R.; Vaszkun, G. Survey of Important Issues in UAV Communication Networks. *IEEE Commun. Surv. Tutor.* **2016**, *18*, 1123–1152. [CrossRef]
8. Hu, B.; Li, X.; Xue, L. A Pilot-Based Integration Method of Ranging and LS Channel Estimation for OFDM Systems. *Drones* **2022**, *6*, 400. [CrossRef]
9. Li, X.; Zeng, X.; Xue, L. Integrated Communication and Measurement System with BOC-Assisted OFDM. *Drones* **2023**, *7*, 14. [CrossRef]
10. Montojo, J.I.; Milstein, L.B. Effects of imperfections on the performance of OFDM systems. *IEEE Trans. Commun.* **2009**, *57*, 2060–2070. [CrossRef]
11. Matin, S.A.; Milstein, L.B. OFDM System Performance, Variability and Optimality With Design Imperfections and Channel Impediments. *IEEE Trans. Veh. Technol.* **2021**, *70*, 381–397. [CrossRef]
12. Kleider, J.E.; Maalouli, G.; Gifford, S.; Chuprun, S. Preamble and embedded synchronization for RF carrier frequency-hopped OFDM. *IEEE J. Sel. Areas Commun.* **2005**, *23*, 920–931. [CrossRef]
13. Bora, A.S.; Singh, T.H.; Huang, P. Digi-FH-OFDM: An all-digital wideband frequency-hopped OFDM system. *Phys. Commun.* **2022**, *52*, 101660. [CrossRef]
14. Huang, Y.; Hu, S.; Wu, G. A TDMA approach for OFDM-based multiuser RadCom systems. *China Commun.* **2023**, *20*, 93–103. [CrossRef]
15. Khawaja, W.; Guvenc, I.; Matolak D.W.; Fiebig, U.; Schneckenburger, N. A Survey of Air-to-Ground Propagation Channel Modeling for Unmanned Aerial Vehicles. *IEEE Commun. Surv. Tutor.* **2019**, *21*, 2361–2391. [CrossRef]
16. Wu, H.; Li, J.; Dai, B.; Liu, Y. Analysis of the Impact of AGC on Cyclic Prefix Length for OFDM Systems. *IEEE Trans. Commun.* **2018**, *66*, 4783–4794. [CrossRef]
17. Wu, H.; Li, J. Analysis and Mitigation of ICI Due to Gain Adjustment in OFDM Systems. *IEEE Access* **2019**, *7*, 21807–21815. [CrossRef]
18. Ijaz, A.; Zhang, L.; Frau, M.; Mohamed, A.; Vural, S.; Quddus, A.U.; Imran, M.A.; Foh, C.H.; Tafazolli, R. Enabling Massive IoT in 5G and Beyond Systems: PHY Radio Frame Design Considerations. *IEEE Access* **2016**, *4*, 3322–3339. [CrossRef]

19. Blumenstein, J.; Bobula, M. Coarse Time Synchronization Utilizing Symmetric Properties of Zadoff-Chu Sequences. *IEEE Commun. Lett.* **2018**, *5*, 1006–1009. [CrossRef]

20. Kang, Y.; Kim, S.; Ahn, D.; Lee, H. Timing estimation for OFDM systems by using a correlation sequence of preamble. *IEEE Trans. Consum. Electron.* **2008**, *54*, 1600–1608. [CrossRef]

21. Abdzadeh-Ziabari, H.; Shayesteh, M. Robust timing and frequency synchronization for OFDM systems. *IEEE Trans. Veh. Technol.* **2011**, *60*, 3646–3656. [CrossRef]

22. Park, B.; Cheon, H.; Kang, C.; Hong, D. A novel timing estimation method for OFDM systems. *IEEE Commun. Lett.* **2003**, *7*, 239–241. [CrossRef]

23. Choi, J.-W.; Lee, J.; Zhao, Q.; Lou, H.-L. Joint ML estimation frame timing and carrier frequency offset for OFDM systems employing time-domain repeated preamble. *IEEE Trans. Wireless Commun.* **2010**, *9*, 311–317. [CrossRef]

24. Abdzadeh-Ziabari, H.; Shayesteh, M. A novel preamble-based frame timing estimator for OFDM systems. *IEEE Commun. Lett.* **2012**, *6*, 1121–1124. [CrossRef]

25. Coulson, A.J. Maximum likelihood synchronization for OFDM using a pilot symbol: Algorithms. *IEEE J. Sel. Areas Commun.* **2001**, *19*, 2486–2494. [CrossRef]

26. Liu, Y.; Yu, H.; Ji, F.; Chen, F.; Pan, W. Robust Timing Estimation Method for OFDM Systems With Reduced Complexity. *IEEE Commun. Lett.* **2014**, *18*, 1959–1962. [CrossRef]

27. Berscheid, B. A Circuit for Low-Complexity Timing Synchronization in OFDM Systems. *IEEE Trans. Circuits Syst. II Express Briefs* **2019**, *66*, 1159–1163. [CrossRef]

28. Hao, X.; Wang, Q.; Yan, X.; Qin, K. A new multiplierless symbol synchronization algorithm for IEEE802.11x WLANs. In Proceedings of the 2014 IEEE 7th Joint International Information Technology and Artificial Intelligence Conference, Chongqing, China, 20–21 December 2014; pp. 176–180.

29. Nie, Q.; Fang, N.; Xu, Z.; Gao, F.; Yang, B. Research on UWB Synchronization Technology and its Implementation in FPGA. *Trans. Beijing Inst. Technol.* **2017**, *37*, 175–179.

30. Zhang, H.; Hou, Y.; Chen, Y.; Li, S. Analysis of Simplified Frame Synchronization Scheme for Burst-Mode Multi-Carrier System. *IEEE Commun. Lett.* **2019**, *23*, 1054–1056. [CrossRef]

31. Thomas, M.C.; Joy, A.T. *Elements of Information Theory*, 2nd ed.; John Wiley Sons, Inc.: Hoboken, NJ, USA, 2006; pp. 305–306.

32. Li, L.; Han, Y.; Chang, Z.; Yang, M. Research and Implementation on OFDM Synchronization Method with Low-Bits Quantization. *Trans. Beijing Inst. Technol.* **2023**, *5*, 526–533.